Study on Mechanical Strength of Cantilever Handrail Joints for Chair

Shuang Li,[b] and Wengang Hu [a,b,*]

Modern solid wood armchairs are developing in the direction of simplicity and lightness, and favored by the market. However, the low mechanical strength of the connecting joint of cantilevered handrails is an issue that needs to be improved. In this study, the armrest joints of a cantilever armchair made by beech (*Fagus orientalis* Lipsky) were examined. To improve the mechanical strength of handrail joints, three novel joints were proposed including dovetail tenon, cross-stepped tenon, and rear plug corner tenon. The finite element analysis (FEA) was used to compare and analyze the five joints to obtain the optimal joint. Finally, experimental tests were conducted to verify the results of the FEA. The novel cross-stepped tenon had better mechanical performance, *i.e*., bending moment capacity and stiffness, than other joints evaluated. The maximum load of the novel cross-stepped tenon was greater than that of the commonly used tenon. In conclusion, the cross-stepped tenon was most suitable for cantilevered handrail joint of chair. This study will contribute to the structural design of modern solid wooden chairs.

DOI: 10.15376/biores.18.1.209-219

Keywords: Cantilever handrail; Tenon and mortise; Finite element analysis; Structure design

Contact information: a: Co-Innovation Center of Efficient Processing and Utilization of Forest Resources, Nanjing Forestry University, Nanjing 210037, China; b: Department of Furniture Design, College of Furnishings and Industrial Design, Nanjing Forestry University, Nanjing 210037, China;
** Corresponding author: hwg@njfu.edu.cn*

INTRODUCTION

To adapt to the sales model of e-commerce, reduce logistics costs, and facilitate mass production, modern solid wood armchairs have been designed to be simple in structure, light in shape, and elegant in appearance. During the use of wooden chairs, the connecting nodes are often subjected to internal and external forces (Eckelman and Haviarova 2006; Fu and Guan 2022). Therefore, the design of the connecting joints of the chair is critically important (Erdil *et al*. 2005; Uysal *et al*. 2015; Xiong *et al*. 2021; Zhou *et al*. 2022a; Li *et al*. 2022; Wang and Yan 2022). Damage to the wooden chair commonly results from the failure or damage of the connecting joint (Eckelman and Haviarova 2006). Traditional tenon and tenon (M&T) joints are widely used in wood furniture frames (Erdil *et al.* 2005), including the leg joints of cantilever armchairs (Boadu and Antwi-Boasiako 2017; Wang *et al.* 2022; Sun and Du 2022). Due to the overall lightness of the chair, the armrest of the chair often has insufficient mechanical strength and is easily damaged due to insufficient size wood materials and adhesive used in joints, as well as the process technology (Cai and Zhou 2022; Hu *et al*. 2022; Zhao *et al*. 2022; Ding *et al*. 2022; Yang *et al*. 2022; Zhou *et al*. 2022b; Zhu *et al*. 2022).

Finite element analysis (FEA) has been used to study the tenon-and-mortise structure for connecting nodes (Kasal *et al*. 2016; Yu *et al*. 2021). A detachable and replaceable non-destructive flat steel sheath reinforcement method can prevent the tenon from being pulled out (Niu and Huang 2020; Krzyżaniak *et al*. 2021; Xia *et al*. 2022), and the initial stiffness and ultimate bearing capacity can be improved significantly (He *et al*. 2021; Okamoto *et al*. 2021; Pan *et al*. 2022a,b). The effects of tenon length, width, and height on the stress distribution and properties of tenon-mortise joints were studied using finite element model (Aejaz *et al.* 2022). The mechanical properties of the designed clearance-penetrating tenon-tenon joint were investigated using a transverse four-frame wood frame, a finite element model with bar elements and rotating springs, and a solid FEM verification method; the resulting deformation characteristics and lateral resistance of the wooden frame were analyzed (He *et al.* 2021). Three reinforcement modes of tenon-jointed wood frames were proposed, and the experiments tested the lateral resistance of tenons in traditional Chinese wood frames. One bay tenon timber frame was subjected to three cycle tests, and three reinforcement methods of steel angle strengthening, wood support and Timo were studied, which were used to provide theoretical basis for the seismic design and reinforcement methods of traditional wood structures (Boadu and Antwi-Boasiako 2017). Many studies have been performed, but the kind of tenon suitable for a cantilever armchair remains unclear.

In this study, the joint applied to the cantilevered handrail chair was investigated to find the suitable mortise and tenon joint in manufacturing. Three novel joints for cantilevered handrail were proposed. Two commonly used joints and the three novel joints were compared using FEA. Finally, experimental tests were conducted to verify the validity of the optimal joint.

EXPERIMENTAL

Materials

The experimental material was beech (*Fagus orientalis* Lipsky) that was stored in a woodworking lab for more than two years in air dry condition. The wood samples were machined using the knot and crack free wood lumbers. The moisture content of the beech wood was 9.46%, and the air-dry density was 0.69 g·cm^{-3}. Table 1 shows the basic mechanical properties of beech wood (Hu *et al.* 2021).

Table 1. Mechanical Parameters of the Beech Wood

Elastic Modulus (MPa)			Poisson's Ratio			Yield Strength (MPa)
E_X	E_Y	E_Z	U_{XY}	U_{YZ}	U_{XZ}	σ_s
12205	1858	774	0.705	0.526	0.705	53.62
E is the elastic modulus (MPa); *U* is Poisson's ratio; X, Y, and Z refer to the longitudinal, radial, and tangential directions of the beech wood, respectively.						

Experimental Design

This study was divided into three steps: 1) three novel joints were designed; 2) finite element models were established to evaluate the three novel joints and two commonly used existing joints through comparing the maximum stress and stiffness; 3) bending tests were conducted to further compare the bending moment capacities of the commonly used rectangle joints and the cross-stepped joints.

Design of the Joints and Specimen Preparation

Mortise and tenon novel design

Two common connecting nodes for commonly used cantilever armchairs were considered. One was rectangle tenon. Their structural forms are shown in Fig. 1a. Rectangle tenon is one of the more common forms of tenon and mortise. Because its mortise and tenon joints were all square, two kinds of square materials were used for vertical and horizontal connection. Commonly used in chair armrests is the closed and not through tenon. The rectangle tenon was usually processed so that the thickness is 0.1 to 0.2 mm smaller than the width of the tenon. When the application section size is large, two or more tenons can be used to improve the connection strength of the tenons.

Another type of tenon structure most widely used in existing armchairs is split oval tenon, as shown in Fig. 1b. Split oval tenon uses separate tenons on both sides to connect the respective mortise. Oval tenon is a variant of rectangle tenon. The difference is that both sides of an oval tenon are semi-cylindrical, and its structural shape is a processed product of modern CNC machine tools. Compared with the whole tenon, the split tenon has higher processing efficiency, higher material utilization, lower processing cost, and easier standardized production, but its tensile strength and bending load are lower. To address the problems of low mechanical strength and easy damage of existing cantilever handrail joints, three novel joints of handrail chairs were proposed to strengthen the mechanical strength of joints.

The first novel joint is a dovetail tenon, as shown in Fig. 1c. The two parts are connected at right angles, and the tenon is in the shape of a ladder with a wide upper and a narrow lower, hence the name "dovetail tenon". Plugging with a concave-convex relationship between materials is the method of connecting dovetail joint and mortise. Its advantage is that the installation steps were simple, and the tenon is only required to be inserted into the mortise from the side. Dovetail tenon processing can be made by hand, dovetail tenon machine, or automatic CNC machining machine. It has a simple structure, convenient manufacture, and low manufacturing cost. After installation, only the joints of the tenon and mortise are exposed, so the external appearance is better.

The second novel joint is a cross-stepped tenon, and its specific form is shown in Fig. 1d. The structural characteristics of the modern cross tenon are referenced by this tenon as a way to improve the cross tenon. One side of the tenon is transformed into a trapezoid. The cross-stepped tenon increased the support point at the front end of the handrail, which is used to increase the force bearing area of the tenon and share the force for the front end of the handrail. Increasing the force-bearing area helped to reduce the maximum stress and avoid the wood grain fracture at the stress point. The cross-stepped tenon requires a variety of platforms with different heights to be processed at the tenon, so there are many processing steps and high processing costs. After the installation, no structural parts are exposed, and the external invisibility was good.

The third novel joint is a rear plug corner joint, and its specific form is shown in Fig. 1e. Reinforcing ribs are used to enhance the compressive and tensile strength of the front end of the armrest, which are connected to the armrest and chair legs respectively through the sliding groove. When installing, the dovetail tenon is connected above the tenon with the dovetail groove of the armrest, and then aligns the dovetail groove of the chair leg with the long dovetail tenon below the plug from bottom to top. During installation, the mortise side of the armrest needs to be chiseled with a mortise face of the same angle as chair leg. The dovetail groove is connected with the mortise and tenon was processed, and the chair leg is placed in the same way. This joint has many processing

procedures, relatively high cost, and a large part of the plug tenon is exposed, so the external appearance is not good.

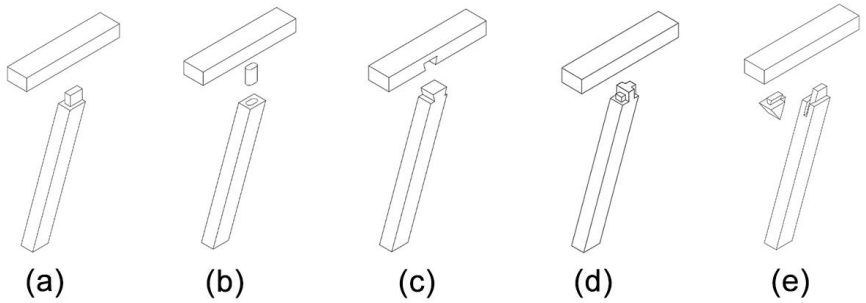

Fig. 1. Cantilevered joints: (a) rectangle tenon; (b) split oval tenon; (c) dovetail tenon; (d) cross-stepped tenon; and (e) rear plug corner tenon

Configurations of the specimen

A square tenon drill was used for tenons, and a flat chisel and hand saw were used for shoulders and stepped tenons. All mortise and tenon joints had the same external size, as shown in Fig. 2a. The detailed size of joints is shown in Fig. 2b.

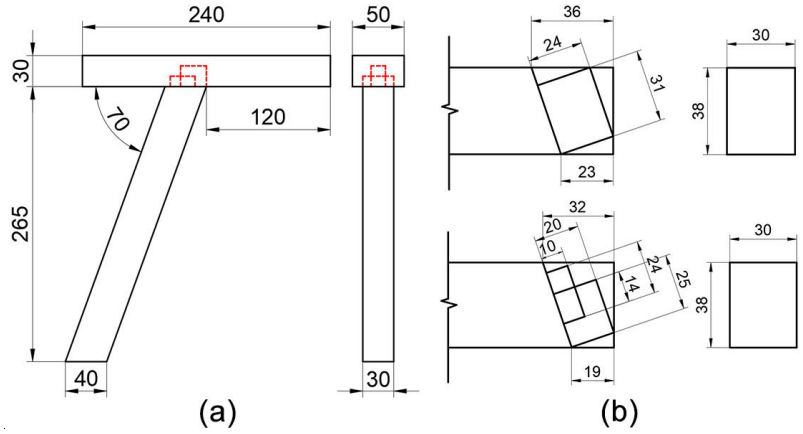

Fig. 2. Dimensions of specimen: (a) T-shaped sample; and (b) joints

Numerical Simulation Method

The establishment of finite element model

The three-dimensional models of the cantilever handrail node were established by SolidWorks, and the finite element simulation experiment was carried out on the node through SolidWorks simulation. The main material of the model was selected as beech. The operation steps for model materials and settings were as follows. First, the model type was linear elastic orthotropic. A plane horizontal with the component direction was selected to ensure that the wood grain was in the same direction. Second, the connection model was global component contact. The contact type was non-penetrating. Thirdly, the geometry was fixed with a fixture, and the end face of bottom of chair leg was selected as the experimental position. Finally, the loading force for external loading was selected, where the normal direction selected the upper edge of the front end of the handrail. The direction selected by the reference plane selected the top surface of the handrail. A load of 800 N was applied downward perpendicular to the reference plane at the normal edge.

Simulation analysis method

The simulation test referred to the experimental method, and the bending test was carried out on the handrail. In this study, all freedoms of chair legs were fixed first. An 800 N load was applied to the end of the handrail vertically. The loading and constraint conditions of the model are shown in Fig. 3, where the purple arrow is the position and direction of the loading force, and the green arrow is the fixed position. The stiffness values were calculated Eq. 1,

$$K=P/\delta \quad (1)$$

where K is stiffness (N/m), P is the constant force acting on the end of handrail (N; in this study, it is 800 N), and δ is the deflection corresponding to force (mm).

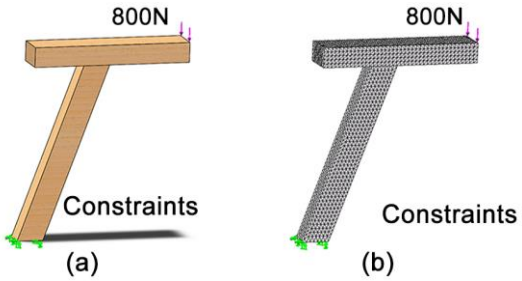

Fig. 3. Finite element model: (a) loads and constraints; and (b) mesh model

Testing Method

Figure 4 shows the device for measuring the bending moment capacity of cantilever joint. The equipment used in this experiment was a universal testing machine (AG-X, 20kN, Shimadzu, Kyoto, Japan). The specimen was fixed on the platform of testing machine with a fixture, and a static load was applied to the specimen at a constant speed in the vertical direction from top to bottom. The position of the fixture to clamp the specimen was 25 mm from the reserved part of the joint of the specimen. To prevent the specimen from hitting the fixture, the loading point was 90 mm away from the joint in horizontal direction. The loading rate was 5 mm/min in the vertical direction. The maximum failure load and corresponding deflection were recorded. The bending moment capacity of joint was calculated using Eq. 2,

$$M = P \cdot L \quad (2)$$

where M is bending moment capacity in N·mm; P is the maximum load in N; L is the force arm corresponding to the load in mm, which was set to 90 mm.

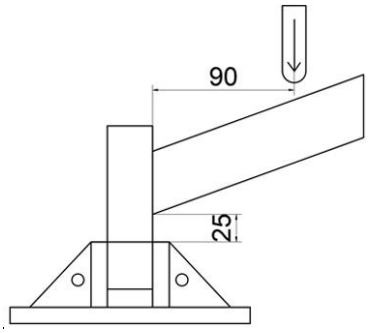

Fig. 4. Setup for testing bending moment capacity of joints

RESULTS AND DISCUSSION

Results of Numerical Simulations

According to the experimental requirements and the parameter settings of the simulation, the finite element simulation analysis was carried out for each structural model. The displacement and maximum stress data in the simulations were collected, and each tenon was analyzed. The deflection and maximum stress of each joint simulation analysis scheme are shown in Figs. 5 and 6. Specifically, the deflection of rectangle tenon was 54.1 mm and the maximum stress was 143 MPa, and the tenon structure had no obvious deformation. The deflection of split oval tenon was 92.9 mm, and a maximum stress was 421 MPa. The mortise and tenon parts of the split tenon were exposed on the side, indicating that the split tenon structure had been deformed. After the loading of 800 N was applied, the deflection of dovetail tenon was 50.6 mm, and the maximum stress was 59.9 MPa. There was no obvious separation between mortise and tenon, and the structure form was most complete. The deflection of the cross-stepped tenon joint was 50.7 mm, and the maximum stress value was 86.2 MPa. In rear plug corner tenon, the deflection of tenon was 57.1 mm, and the maximum stress was 367 MPa. The long dovetail joint of rear plug corner tenon had compression deformation. The rear plug also had obvious deflection.

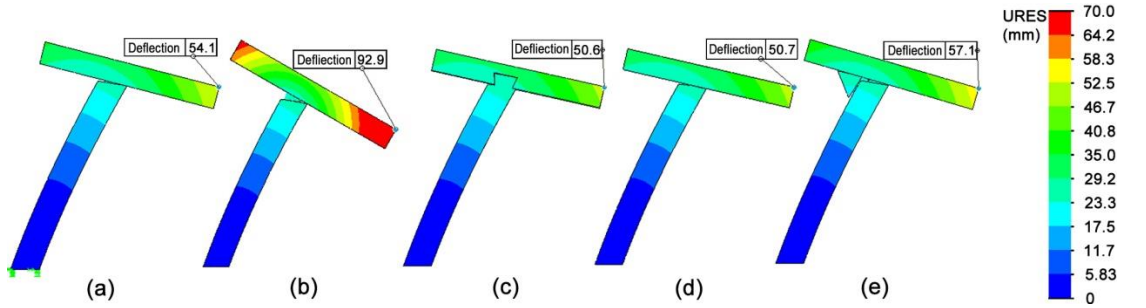

Fig. 5. Displacement distributions of commonly used and novel joints: (a) rectangle tenon; (b) split oval tenon; (c) dovetail tenon; (d) cross-stepped tenon; and (e) rear plug corner tenon

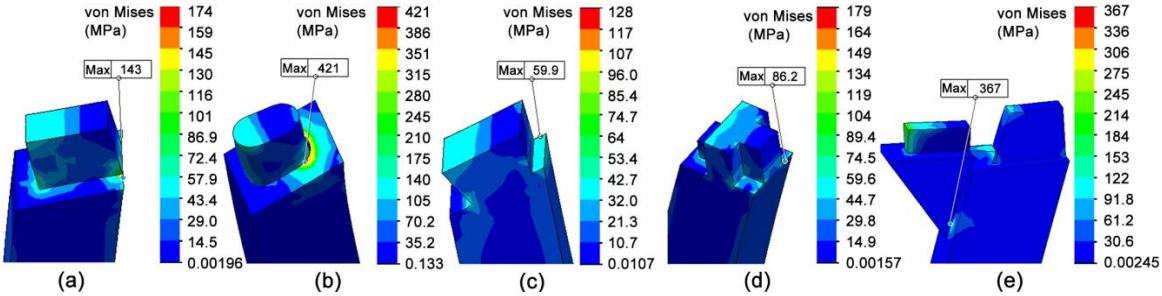

Fig. 6. Stress distributions of commonly used and novel joints: (a) rectangle tenon; (b) split oval tenon;(c) dovetail tenon; (d) cross-stepped tenon; and (e) rear plug corner tenon

Combined with the finite element simulation experiment, the displacement and stress of the five joints were obtained, and the stiffness value of each joint was calculated using Eq. 1. Table 2 shows the results of stiffness and stress of the commonly used rectangle joints and the four novel joints proposed in this study. The mechanical strength of the dovetail tenon was the highest, and the stiffness and maximum stress were 15.8 N/m

and 59.9 MPa, respectively. The stiffness and the maximum stress of the cross-stepped tenon were 15.8 N/m and 86.2 MPa, respectively, which were consistent with the stiffness of the dovetail tenon. The mechanical strength of the split oval tenon was the worst, with the stiffness and maximum stress values of 14.0 N/m and 367 MPa.

Table 2. Stiffness and Maximum Stress of Commonly Used and Novel Joints

Joints	Stiffness (N/mm)	Stress (MPa)
Rectangle Tenon	14.78	143
Split Oval Tenon	8.61	421
Dovetail Tenon	15.81	60
Cross-Stepped Tenon	15.78	86
Rear Plug Corner Tenon	14.01	367

For cantilever handrail joints, high stiffness was needed to resist the force acting on the end. According to the above numerical simulation results, the mechanical strength of the tenon-and-mortise structure was analyzed. The best solution among the above five solutions was cross-stepped tenon. Cross-stepped tenon exhibited good mechanical properties and was close to dovetail tenon in terms of maximum stress and displacement. However, cross-stepped tenon had no structural exposure compared to dovetail tenon, and had better external aesthetics. Among the commonly used joints, the rectangular tenon had the best mechanical strength. Further experimental study was based on these two tenons to validate if the cross-stepped tenon has better strength performance when used in cantilever handrail chair.

Experimental Results

Figure 7a shows the typical load-deflection curves of cantilever handrail jointed by cross-stepped tenon and commonly used rectangle tenon. Figure 7b shows the average maximum bending load of them with the values of 730.7 N and 896.4 N. The bending moment of cross-stepped tenon and rectangle tenon cantilever handrail were 65800 N·mm and 80700 N·mm, respectively, which were calculated using Eq. 2. In order to further compare the strength of them, analysis of variance (ANOVA) based on general linear mode (GLM) and least square difference (LSD) method were conducted at 5% significance level. The analysis results indicated that the mechanical strength of cross-stepped tenon joint was significantly higher than rectangle tenon joint. Thus, it can be concluded that the cross-stepped joint performed better than rectangle joint when used in cantilever handrail joint using FEM and experimental test.

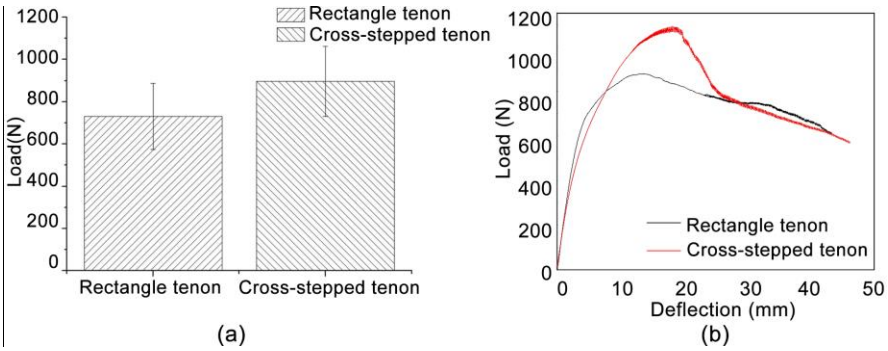

Fig. 7. Experimental results: (a) maximum failure load of the specimens; and (b) load stroke curve of bending strength

Failure modes analysis

Figure 8 shows the failure form of rectangle tenon in the commonly used joints. The mortise and tenon of the test piece were separated to observe the degree of internal damage. The tenon shoulder and the right side of the tenon were squeezed. In Fig. 8b, the squeezed part on the upper left of the tenon had been severely fractured. In the lower right part of Fig. 8c, the crushed part of the mortise is opposite to the direction of the wood grain, and the damage degree is relatively small.

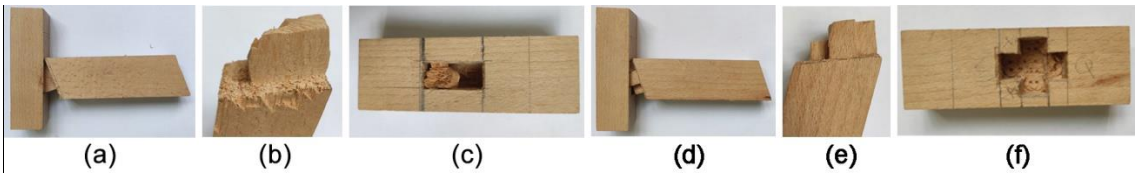

Fig. 8. Failure modes of rectangle tenon: (a) overall; (b) tenon; and (c) mortise, and cross-stepped tenon: (d) overall; (e) tenon; and (f) mortise

As shown in Fig. 8, the failure mode of specimen in novel cross-stepped tenon was squeezed at the tenon and the mortise in the right direction. The mortise and tenon of the test piece were separated, and the degree of internal damage was observed. The upper left part of the tenon was deformed by extrusion (Fig. 8e). The middle of the tenon was partially broken at the extrusion point of the mortise.

The numerical and experimental results showed that the tenon-and-mortise structure proposed in this study for the joint of chair armrests had better mechanical strength and stability. However, only the finite element method had been used to compare and analyze the maximum stress and magnitude relationship at failure between the commonly used structures and the novel structures. Further research will pay attention to a wider variety of connection methods between furniture components to increase the mechanical properties of connection nodes more efficiently in furniture frames.

CONCLUSIONS

In this study, the bending strength of armrest joints of cantilever armchair were studied using finite element method (FEM) and experimental tests to improve the mechanical strength of handrail joints. Following conclusions were drawn.

1. Three novel joints, including dovetail tenon joint, cross stepped tenon joint and the rear corner tenon joint were proposed to improve the bending moment capacity of the cantilever handrail joint.
2. The finite element model was established and used to simulate and compare the novel joints and commonly used rectangle joints in maximum stress and stiffness, which indicated that the cross-stepped tenon performed better than the other joints evaluated considering both strength and external appearance of tenon.
3. The experimental tests showed that the bending moment capacity of the cross-stepped tenon joint had better performance than the commonly used rectangle joints in cantilever handrail with the bending moments of 80700 N·mm and 65800 N·mm, respectively.

This study proposed three types of new joints used in cantilever armrest chair, which were analyzed and compared with the commonly used rectangle joint, and validated to be having higher strength. This study will contribute to design of modern cantilever armrest chair, and make the joint more reliable in strength.

ACKNOWLEDGMENTS

This study was partially supported by the Scientific Research Foundation of Nanjing Forestry University (GXL2019074) and partially supported by the Project from International Cooperation Joint Laboratory for Production, Education, Research and Application of Ecological Health Care on Home Furnishing.

REFERENCES CITED

Aejaz, A., Dar, A. R., and Bhat, J. (2022). "Numerical study on the nonlinear behavior of full-scale timber framed joints," *Practice Periodical on Structural Design and Construction* 26(1). DOI: 10.1061/(ASCE)SC.1943-5576.0000539

Boadu, K., and Antwi-Boasiako, C. (2017). "Assessment of the bending strength of mortise-tenon and dovetail joints in leg-and-rail construction using *Klainedoxa gabonensis Pierre Ex Engl.* and *Entandrophragma cylindricum (Sprague) Sprague*," *Wood Material Science & Engineering* 12(4), 242-250. DOI: 10.1080/17480272.2016.1174883

Cai, C., and Zhou, F. (2022). "Sorption characteristic of thermally modified wood at varying relative humidity," *Forests* 13, article 1687. DOI: 10.3390/f13101687

Ding, T., Yan, X., and Zhao, W. (2022). "Effect of urea–formaldehyde resin–coated colour–change powder microcapsules on performance of waterborne coatings for wood surfaces," *Coatings* 12, article 1289. DOI: 10.3390/coatings12091289

Eckelman, C. A., and Haviarova, E. (2006). "Performance tests of school chairs constructed with round mortise and tenon joints," *Forest Products Journal* 56(3), 51-57.

Erdil, Y. Z., Kasal, A., Eckelman, C. A. (2005). "Bending moment capacity of rectangular mortise and tenon furniture joints," *Forest Products Journal* 55(12), 209-213.

Fu, W., and Guan, H. (2022). "Numerical and theoretical analysis of the contact force of oval mortise and tenon joints concerning outdoor wooden furniture structure," *Wood Science and Technology* 56(4), 1205-1237. DOI: 10.1007/s00226-022-01395-w

He, J., Yu, P., Wang, J., Yang, Q., Han, M., and Xie, L. (2021). "Theoretical model of bending moment for the penetrated mortise-tenon joint involving gaps in traditional timber structure," *Journal of Building Engineering* 42. DOI: 10.1016/j.jobe.2021.103102

Hu, J., Liu, Y., Xu, W., Wu, Z., and Pan, X. (2022). "Effects of preparation and self-assembly of poly (styrene-acrylic acid) (P(St-AA)) microspheres upon constructed photonic crystals with structural color on wood surfaces," *Coatings* 12, article 1520. DOI: 10.3390/coatings12101520

Hu, W., Chen, B., and Zhang, T. (2021). "Experimental and numerical studies on mechanical behaviors of beech wood under compressive and tensile states," *Wood*

Research 66(1), 27-37. DOI: 10.37763/wr.1336-4561/66.1.2738

Kasal, A., Smardzewski, J., Kuşkun, T., and Erdil, Y. Z. (2016). "Numerical analyses of various sizes of mortise and tenon furniture joints," *BioResources* 11(3), 6836-6853. DOI: 10.15376/biores.11.3.6836-6853

Krzyżaniak, Ł., Kuşkun, T., Kasal, A., and Smardzewski, J. (2021). "Analysis of the internal mounting forces and strength of newly designed fastener to joints wood and wood-based panels," *Materials* 14(23), article 7119. DOI: 10.3390/ma14237119

Li, W., Yan, X., and Zhao, W. (2022). "Preparation of crystal violet lactone complex and its effect on discoloration of metal surface coating," *Polymers* 14, article 4443. DOI: 10.3390/polym14204443

Niu, X., and Huang, J. (2022). "Research on backrest modeling of Ming-style furniture with full carving using technology of eye tracking," *Journal of Forestry Engineering* 7(3), 200-206. DOI: 10.13360/j.issn.2096-1359.202108018

Okamoto, S., Nakatani, M., Akiyama, N., Tanaka, K., and Mori, T. (2021). "Verification of the shear performance of mortise and tenon joints with top and bottom notches at the beam end," *Journal of Wood Science* 67, 47. DOI: 10.1186/s10086-021-01979-3

Pan, P., Yan, X., and Peng, W. (2022a). "Tung oil microcapsules prepared with different emulsifiers and their effects on the properties of coating film," *Coatings* 12, article 1166. DOI: 10.3390/coatings12081166

Pan, W., Yan, X., and Zhao, W. (2022b). "Effect of coating process of photochromic and thermochromic composite microcapsules on coating properties for basswood," *Coatings* 12, article 1246. DOI: 10.3390/coatings12091246

Sun, B., and Du, H. (2022). "Research on style cognition of Neo-Chinese armchair based on image scale," *Journal of Forestry Engineering* 7(5), 190-196. DOI: 10.13360/j.issn.2096-1359.202202013

Uysal, M., Haviarova, E., and Eckelman, C. A. (2015). "A comparison of the cyclic durability, ease of disassembly, repair, and reuse of parts of wooden chair frames," *Materials & Design* 87, 75-81. DOI: 10.1016/j.matdes.2015.08.009

Wang, L., Han, Y., and Yan, X. (2022). "Effects of adding methods of fluorane microcapsules and shellac resin microcapsules on the preparation and properties of bifunctional waterborne coatings for basswood," *Polymers* 14, article 3919. DOI: 10.3390/polym14183919

Wang, L., and Yan, X. (2022). "Preparation of resin-coated waterborne coating microcapsules and its effect on the properties of waterborne coating for wood surfaces," *Coatings* 12, article 1394. DOI: 10.3390/coatings12101394

Xia, Y., Yan, X., and Peng, W. (2022). "Preparation of cellulose modified wall material microcapsules and its effect on the properties of wood paint coating," *Polymers* 14, article 3534. DOI: 10.3390/polym14173534

Xiong, X., Lu, G., and Lu, D. (2021). "Research on children's customized furniture design based on group technology," *Applied Sciences* 11, article 11371. DOI: 10.3390/app112311371

Yang, Z., Han, Y., Peng, W., Wang, L., Yan, X. (2022). "Effect of fluorane microcapsule content on properties of thermochroic waterborne topcoat on *Tilia europaea*," *Polymers* 14, article 3638. DOI: 10.3390/polym14173638

Yu, M., Sun, D., Zou, W., Wang, Z., Jiang, X., Yao, L., and Kong, J. (2021). "Mechanical analysis of new Chinese style wood chairs using ANSYS," *Journal of Forestry Engineering* 6(3), 178-184. DOI: 10.13360/j.issn.2096-1359.202006021

Zhao, Z., Zhang, X., Lin, Q., Zhu, N., Gui, C., and Yong, Q. (2022). "Development and

investigation of a two-component adhesive composed of soybean flour and sugar solution for plywood manufacturing," *Wood Material Science & Engineering* 16, article 2086067. DOI: 10.1080/17480272.2022.2086067

Zhou, C., Huang, T., Luo, X., Kaner, J., and Fu, X. (2022a). "Cluster analysis of kitchen cabinet operation posture based on OpenPose technology," *International Journal of Industrial Ergonomics* 91, article 103352. DOI: 10.1016/j.ergon.2022.103352

Zhou, C., Huang, T., Luo, X., Kaner, J., Fu, X. (2022b). "Recognition and analysis of an age-friendly intelligent sofa design based on skeletal key-points," *International Journal of Environmental Research and Public Health* 19(18), article 11522. DOI: 10.3390/ijerph191811522

Zhu, Z., Buck, D., Wang, J., Wu, Z., Xu, W., and Guo, X. (2022). "Machinability of different wood-plastic composites during peripheral milling," *Materials* 15(4), article 1303. DOI: 10.3390/ma15041303

Article submitted: July 28, 2022; Peer review completed: October 22, 2022; Revised version received: October 22, 2022; Accepted: November 1, 2022; Published: November 8, 2022.
DOI: 10.15376/biores.18.1.209-219